



# Magnetocrystalline anisotropy of small CoPt binary alloy metal clusters: interplay between structure, chemical composition, and spin-orbit coupling

J. L. Ricardo-Chávez · M. Muñoz-Navia ·  
P. Ruiz-Díaz

Received: 31 March 2020 / Accepted: 21 May 2020 / Published online: 18 July 2020  
© Springer Nature B.V. 2020

**Abstract** The ground-state magnetic properties of  $\text{Co}_n\text{Pt}_m$  binary alloy clusters of size  $N = n + m \leq 9$  are studied systematically as a function of size, composition, and chemical order in the framework of the generalized gradient approximation (GGA) to density functional theory (DFT). Interestingly, strong cluster-size and chemical-composition dependence exhibiting substantial values (0.4–22 meV/atom) in the magnetic anisotropy energy (MAE) are revealed. Such behavior crucially depends on the Pt moments induced by the proximity to Co, and on the resulting spin-orbit interactions at the Pt atoms. Moreover, we show that the MAEs and direction of magnetization can be tuned to some extent by varying the Pt concentration showing spin reorientations and the easy axis

of magnetization is cluster size dependent. A thorough cluster-geometry optimizations together with a collinear and noncollinear magnetic moment arrangement sampling including the spin-orbit coupling are carried out to identify the ground-state and the low-lying structures. The relative directions between Co and Pt magnetic moments induced by spin-orbit interaction show an early tendency to arrange the magnetic moments along with Co and Pt layers in a way resembling the  $\text{L1}_0$  phase with tetragonal crystal lattice which can be appreciated in the clusters having  $N \geq 5$  atoms. Our results show that planar-like structures are preferred in small cluster sizes ( $N \leq 4$  atoms) while for  $N \geq 5$  tend to form three-dimensional core-shell compact structures with a composition around 50/50% ordering maximizing the number of Co-Pt bonds. The average magnetic moment per atom  $\bar{\mu}_T$  increases approximately linearly with Co content and important enhancement of the local Co moments is observed as a result of Pt doping for  $n + m \leq 4$ . This is mainly a consequence of the increase in the number of Co  $d$  holes due to Co to Pt charge transfer. Finally, our results show important spin and orbital moments induced at the Pt atoms as well as significant orbital moments at the Co atoms.

J. L. Ricardo-Chávez  
Facultad de Ciencias Físico-Matemáticas  
and Laboratorio Nacional de Supercómputo, Benemérita  
Universidad Autónoma de Puebla, Calle 4 Sur No. 104, Col.  
Centro, C. P. 72000, Puebla, Mexico

M. Muñoz-Navia  
Universidad de La Ciénega del Estado de Michoacán  
de Ocampo, Avenida Universidad 3000, Col. Lomas  
de la Universidad, Sahuayo, Michoacán, Mexico

P. Ruiz-Díaz (✉)  
Instituto de Física, Universidad Autónoma de San Luis  
Potosí, Álvaro Obregón, 78000 San Luis Potosí, Mexico  
e-mail: prudi@ifisica.uaslp.mx

**Keywords** CoPt core-shell alloy clusters ·  
Magnetic anisotropy · Ab initio calculations ·  
Binary nanoalloys · Modeling and simulation

## Introduction

Magnetic nanoalloys have been the subject of numerous experimental and theoretical studies in the last years (Bansmann et al. 2005; Tamion et al. 2009; Penuelas et al. 2009; Entel and Gruner 2009; Gruner et al. 2008; Sahoo et al. 2010; Yanagisawa et al. 1983; Liou et al. 1999; Maret et al. 1996; Gruner and Entel 2009; Rollmann et al. 2008; Knickelbein 2007; Yin et al. 2007; Zitoun et al. 2002; Muñoz-Navia et al. 2009). This subject is currently attracting considerable attention from both fundamental and technological perspectives. For example, for high-density magnetic recording, one would like to be able to develop magnetic nanoparticles that combine both high saturation magnetization (MS) and large magnetic anisotropy energy (MAE). This can indeed be achieved by starting from a ferromagnetic (FM) 3d transition metal (TM) and by associating it with a second heavier element that displays a stronger spin-orbit coupling and a potentially significant contribution to the total magnetization. Quite generally, 4d and 5d metals appear as very good candidates for this purpose. The magnetic characteristics of alloys are determined not only by their structure and composition, but also by the relative order of its constituents within the system, making possible to present countless different properties. In this way, by alloying, one could generate a variety of materials with complementary qualities in order to fulfill specific requirements for different applications. Low-dimensional magnetism of alloys has therefore recently gained the attention of basic and applied research since its underlying mechanisms and the way they develop to reach the bulk properties remain unclear. Hence, a thorough understanding of the low-dimensional magnetism of TM and its alloys would allow not only to take advantage of their properties but also to even design new materials with the desired properties (Bansmann et al. 2005; Zitoun et al. 2002; Muñoz-Navia et al. 2009; Plumer and van Ek 2001; Sun et al. 2000).

Co-Pt alloys are particularly appealing since Pt is a highly polarizable material despite being non-magnetic in bulk. The importance of combining Co with Pt was already demonstrated for Co films on Pt substrates many years ago. Indeed, Co/Pt thin films have been found to present strong perpendicular magnetic anisotropy (Maret et al. 1996; Yanagisawa et al. 1983; Maret et al. 1997; Thomson et al. 2006; Hellwig

et al. 2007; Shaw et al. 2007; Gradmann 1993; Vaz et al. 2008; Gambardella et al. 2003; Yu et al. 2000; Valvidares et al. 2010). Moreover, experiments on CoPt nanoparticles have shown that alloying Co with Pt should be an effective way to combine large magnetic moments with large magnetic anisotropy energy (Bansmann et al. 2005; Zitoun et al. 2002; Muñoz-Navia et al. 2009). The ensemble of these results demonstrates that the diversity of local chemical environments present in these nanoalloys and the competition between Co–Co, Co–Pt, and Pt–Pt effective exchange couplings would lead us to expect very interesting size and structural dependence of the magnetic distribution as well as on the magnetic anisotropy.

The electronic and magnetic properties of Co-Pt nanoalloys have been actively studied for several years, both experimentally (Bansmann et al. 2005; Penuelas et al. 2009; Tamion et al. 2009) and theoretically (Entel and Gruner 2009; Gruner et al. 2008; Entel and Gruner 2009; Sahoo et al. 2010). For example, Favre et al. (2006) studied experimentally the structural and magnetic properties of CoPt clusters ( $\simeq 300$  atoms). By using a simple core-shell model, Jamet et al. (2001) suggest that their cobalt nanoparticles embedded in a platinum matrix were composed by a cobalt core and an alloyed interface. Dupuis et al. (2004) studied Co-based (CoPt) clusters on different matrices and noticed the importance of surface/interface effects on the magnetic properties and the MAE. Ruiz-Díaz et al. (2018) showed that the magnetic properties of CoPt nanoparticles are strongly sensible to external stimuli. They found for medium-sized clusters that both the direction of magnetization and the magneto-crystalline anisotropy of these binary compounds further stabilize upon charge(hole)-doping. Kumbhar et al. (2001) observed an increase of the blocking temperature as Pt content increases for CoPt and CoPt<sub>3</sub> clusters coated with Au. One important characteristic of the CoPt clusters is the segregation of the components for rich Pt composition (Moskovkin et al. 2007). This was confirmed by large-scale first principles theoretical studies on CoPt clusters by Gruner et al. (2009, 2008), who showed a tendency of the Pt atoms toward the surface and energetically favored multiply twinned morphologies. In addition, the same group calculated the surface energies of ordered CoPt, and obtained remarkable low surface energy of Pt terminated (111) facets (Dannenberg et al. 2009). Feng et al. (2007) investigated the

structural and magnetic properties of small  $\text{Co}_x\text{Pt}_{1-x}$  clusters for  $x = 0.5$ . They studied structures composed of  $n$  Co–Pt units ( $n \leq 5$ ) and obtained three-dimensional structures with enhanced cobalt moments by doping and a slight increase of the Pt magnetic moments with favored Co–Co aggregation.

Despite the intense research activity, to our knowledge, there is no available study in which magnetism, structure, and chemical order are considered on the same electronic level, in particular on determining the magnetocrystalline anisotropy energies of small CoPt binary alloy metal clusters. It is the purpose therefore of this work to investigate the magneto-anisotropic properties of the most stable structures as a function of the cluster size and chemical composition and meticulously determine the MAE and its behavior of small alloy CoPt clusters having  $N \leq 9$  atoms. To this aim, we perform an exhaustive exploration of the various possible spin configurations and chemical orders within the cluster taking into account geometry relaxation and the structural dependence on the same footing. The remainder of the paper is organized as follows. First, the theoretical background is briefly recalled providing specific details of the calculations. Then, the magnetic behavior of each cluster size as a function of composition and chemical order and some general trends are discussed. Later, the magneto-anisotropic properties of alloy CoPt clusters are analyzed. Finally, some general conclusions are outlined.

## Methodology

The calculations are performed in the framework of Hohenberg-Kohn-Sham's density functional theory (Hohenberg and Kohn 1964; Kohn and Sham 1965) as implemented in the Vienna ab initio simulation package (VASP) (Kresse and Furthmüller 1996; Kresse and Hafner 1993). This computer code solves the spin-polarized Kohn-Sham (KS) equations (Hohenberg and Kohn 1964; Kohn and Sham 1965) in an augmented plane-wave basis set by using the projector augmented wave (PAW) method (Blöchl 1994; Kresse and Joubert 1999), which is an approximate all-electron approach with frozen cores. For  $3d$  ( $5d$ ) TMs, the electronic and magnetic properties are accurately described by considering the  $3d$ ,  $4s$ , and  $4p$  ( $5d$ ,  $6s$ , and  $6p$ ) electrons as valence states (Blöchl 1994; Kresse and

Joubert 1999). The exchange and correlation effects are treated within the generalized-gradient approximation (GGA) by using the Perdew-Burke-Ernzerhof (PBE) functional (Perdew et al. 1992, 1996). The clusters are placed inside of a simple cubic supercell whose dimensions are such that the interactions between neighboring images are negligible. In this work, this criterion was achieved by separating by at least  $12\text{\AA}$ . The KS wave functions in the interstitial region are expanded in a plane wave basis set with a kinetic energy cutoff of 575 eV. For the considered clusters, the total energy is converged within less than 1 meV/atom. For metallic-like systems, one often finds very rapid variations of states close to the Fermi level that may cause a poor convergence of relevant physical quantities such as the total energy. Therefore, a smearing of the KS levels is introduced in order to improve numerical stability. We have used a Gaussian smearing method (Mermin 1965; Vita and Gillan 1992) with a very small final standard deviation  $\sigma = 0.01$  eV, which keeps the entropy of the non-interacting KS gas below  $10^{-5}$  eV/K-atom. The WS sphere radii for Co (Pt) of 1.302 Å (1.455 Å) respectively were considered for the integration of the local properties. The calculation of all properties is carried out by considering only the  $\Gamma$ -point in reciprocal space since we are dealing with isolated clusters.

## Structural optimization of $\text{Co}_n\text{Pt}_m$ clusters and calculation of the magnetic properties

The geometry optimization is performed by using the conjugate-gradient and quasi-Newton methods until all the forces on each atom are less than  $5 \text{ meV}/\text{\AA}$ . In order to investigate thoroughly all the magnetic solutions of the Kohn-Sham equations, a large number of different spin configurations have been considered as starting points for the numerical iterations. The energy landscape of the clusters is comprehensively explored by considering a large, complete, and most possibly unbiased set of initial structures that include not only the representative cluster geometries or topologies, but also all relevant chemical orders or distributions of the Co and Pt atoms for a given composition. In this work, we sample the different cluster topologies in the framework of graph theory by generating all possible graphs for  $N \leq 9$  atoms as described elsewhere. For each given cluster size  $N$  and topology, we investigate all compositions of  $\text{Co}_m\text{Pt}_n$  including the pure

$\text{Co}_N$  and  $\text{Pt}_N$  limits. Moreover, we take into account all possible non-equivalent distributions of the  $m$  Co and  $n$  Pt atoms within the cluster. In this way, any a priori assumption on the chemical order is avoided.

First of all, a systematic exploration of collinear magnetic spin arrangements is carried out by varying the total spin moment  $S_z$  in its full range  $0 < S < 3N$  followed by a test of different noncollinear spin configurations (typically 20) for determining the true ground-state magnetic solution. It is important to remark that in all cases, i.e., for all  $S_z$  and for all starting magnetic configurations, the geometry has been optimized following the forces resulting from the self-consistent solution of the KS equations. This is the relevant method in order to determine the most stable structure, total spin moment  $S_z$ , and the associated magnetic order, since relaxations of geometric, electronic, and magnetic degrees of freedom need to be treated on the same footing. However, notice that the procedure precludes one from obtaining interesting complex spin arrangements which, though corresponding to the electronic ground state for a given fixed structure, would yield non-vanishing interatomic forces.

In addition, an analysis using Bader atomic cells (Henkelman et al. 2006; Sanville et al. 2007; Tang et al. 2009) is used in order to check the accuracy of the values of the electronic charge. We found that in all cases the Bader calculations give the same trends as the PAW method. Once the optimization with respect to structural and magnetic degrees of freedom is achieved, we derive the binding energy per atom  $E_B = [mE(\text{Co}) + nE(\text{Pt}) - E(\text{Co}_m\text{Pt}_n)]/N$  in the usual way by referring the total energy  $E$  to the corresponding energy of  $m$  Co and  $n$  Pt isolated atoms.

### Magnetocrystalline anisotropy

The magnetocrystalline anisotropy energy (MAE) is a very sensitive quantity which requires to be treated with extreme care since for clusters in the gas phase is usually of the order of just a few meVs. Therefore, in order to determine the magnetocrystalline energy of the isolated clusters, relativistic calculations taking into account the *spin-orbit* interaction (SOC) are carried out with a tighter criterion in the electronic energy ( $\Delta E = 10^{-7}$  eV between two successive electronic steps). Such a strict criterion is crucial for calculating reliable MAEs. We should point out that all the

calculations for determining the MAE of the clusters are fully self-consistent (relativistic) calculations which allow us to treat all the interactions on the same footing.

We perform a complete relaxation of the systems, in the relativistic framework of the two components (spinors) of the spin-orbit interaction as implemented in the VASP code, namely, an initial direction of the magnetic moments is given and the system relaxes itself, both structurally and magnetically (i.e., the direction of the magnetic moments can rotate until a stable magnetic solution is found). The obtained directions of magnetization correspond to a true total-energy minima. Each of these minima has sort of an attractive potential in such a way that if the system is perturbed and such perturbation is unable to bring the system out of the potential, the system will converge again to the same minimum upon relaxation. From this point of view, we are not obtaining the MAE of the system in the strict sense, because both the structure and the magnetic direction vary. We calculate the energy differences between stable structures and directions of magnetization.

Even more, as the cluster size increases, to infer the truly easy and hard axes of magnetization is not straightforward due to the symmetry-breaking imposed for the cluster geometry. Therefore, there is, in general, no formal way to guess a priori the direction of the easy- and hard-magnetization axes without mapping the entire energy landscape of the system as a function of the direction of magnetization. In this way, it would be easy to locate the minima, saddle points, and minimum energy paths (MEP) among them. In this paper, we follow a simpler approach. We determine self-consistently three magnetization directions, not necessarily perpendicular among them and not related in general to the global easy and hard axes, but that could be easily explored experimentally by adjusting the direction of the magnetic field. So, the reported magnetic anisotropy values correspond to energy differences between these local energy minima and serve only as lower bond estimations of the energy needed to switch the magnetization between these directions. We are aware that, strictly speaking, the switching energy would be the activation energy to surmount the barrier separating two neighbor minima, but we cannot claim the energy minima we have determined are connected by a MEP.

Due to the large value of the Pt spin-orbit coupling, strong structural effects have been reported in pure Pt clusters having  $N \leq 6$  atoms (Błoński et al. 2011). Nonetheless, in our study, the alloy CoPt clusters are the ground-state structures in all the cases and the structural effects considering the spin-orbit interaction turn to be meaningless. Namely, the ground-state structures remain essentially the same as in the scalar relativistic (SR) calculations (SOC = 0). Moreover, the changes in the bond lengths  $d_{i,j}$  and in the average spin moments  $\mu^S$  resulting from the SOC interactions are also very small:  $|\mu^{SOC} - \mu^{SR}| \approx 0.01 \mu_B$  and  $|d^{SOC} - d^{SR}| \approx 0.01 \text{ \AA}$ . On the other hand, the SOC interactions are key for the onset of easy(hard) axes of magnetization, as well as for the orbital contribution to the total cluster magnetic moment. Therefore, all the binding energies, magnetic moments, and bond distances reported in the present work include the spin-orbit interaction (relativistic approach).

## Results and discussion

In this section, we present our results regarding the ground-state structure, binding energy, chemical composition dependence, magnetic spin and orbital moments, and MAEs of  $\text{Co}_m\text{Pt}_n$  clusters having  $N = m + n \leq 9$  atoms. The discussion is organized in separate “Dimers”–“Pentamers” for each  $N$ , starting from the dimer. From the dimers  $N = 2$  each concentration and chemical order, the structural relaxation is carried out by taking into account all the possible topologies, allowed by graph theory, as starting geometrical configurations.

Although the potential advantages of alloying magnetic  $3d$  elements with highly polarizable  $5d$  elements at the nanoscale can be grasped straightforwardly, the problem involves a number of serious practical challenges. Different growth or synthesis conditions can lead to different chemical orders, which can be governed not just by energetic reasons but by kinetic processes as well. For instance, one may consider segregated clusters with either a  $5d$  core and a  $3d$  outer shell or vice versa. Post-synthesis manipulations can induce different degrees of intermixing, including for example surface diffusion or disordered alloys. For this reason, we give the results for the two most stable isomers for each chemical concentration. Finally, our results are compared with previous calculations whenever available.

## Structural stability

We start first by discussing the structural stability of the clusters as a function of the size and chemical composition. As can be seen in Fig. 1, we can clearly appreciate that the cluster further stabilizes as both the size and the Pt doping are increased. The binding energies range from 1.5 eV/atom for the pure Co dimer to approximately 3.25 eV/atom for the pure  $\text{Pt}_6$  cluster respectively. On the other hand, for a fixed cluster size, one observes upon Pt doping that the binding energy begins to increase linearly until reaching a maximum for an intermediate doping value (between 2 and 4 atoms of Pt, depending on the cluster size). Then, the energy slightly decreases until reaching the binding energy of the pure clusters of Pt (roughly 5% lower). Only in the case of  $N = 4$ , the decrease in the energy is more noticeable ( $\Delta E \approx 0.5$  eV). For sizes greater than  $N = 4$ , the maximum of the stability curves is shifted to compositions above 50% of Pt, indicating a competition for the stability of structural phases CoPt and  $\text{CoPt}_3$ .

## Dimers

To infer some useful trends on charge transfers, magnetic order, and relative strength on the various types of bonds (Co–Co, Co–Pt, and Pt–Pt) which are found

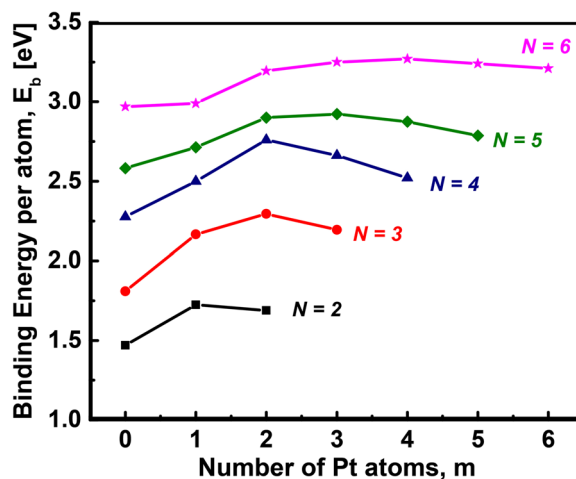


**Fig. 1** Relativistic calculations including the spin-orbit coupling of the binding energy per atom of  $\text{Co}_n\text{Pt}_m$  ( $n + m \leq 6$ ) as a function of Pt doping  $m$ . Energies correspond to the easy axis of the magnetization

in larger alloy clusters, we first present the results for the dimers.

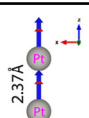
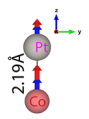
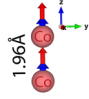
Our results for Co–Pt dimers are summarized in Table 1. We obtain that the Co–Pt bond yields the highest binding energy, followed by the Pt–Pt bond, the Co<sub>2</sub> bond being the weakest. However, notice that the Pt–Pt binding energy is very close to that of Co–Pt bond ( $\Delta E = 34$  meV). The binding energy  $E_B = 1.47$  eV obtained for Co<sub>2</sub> is in fair agreement with the non-local density functional calculations using the ADF code (Fan et al. 1997) 1.425 eV and with the LDA calculations of Barden et al. (2000) and far from the results of Pereiro et al. (2001) who found  $E_B = 0.87$  eV. However, notice that these values remain somewhat larger than the experimental value  $E_B^{expt} \leq 1.32$  eV (Hales et al. 1994). In the case of Pt<sub>2</sub>, our result,  $E_B = 1.69$  eV and interatomic distance  $d_e = 2.377$  Å, is in qualitative agreement with previous GGA calculations performed by Zarechnaya et al. (2008) and by full-relativistic calculations (Anton et al. 2002) (1.65 and 1.56 eV respectively). These are close to the experimental value (Airola and Morse 2002),  $E_B(\text{Pt}_2) = 1.57$  eV. Notice that our results are in agreement with recent non-relativistic calculations (Błoński et al. 2011) in small Pt clusters by using the VASP code. In the same work, Blonski et al. (2011) have also shown that if spin-orbit interactions are taken into account, the Pt–Pt bond length increases slightly up to 2.38 Å which is the same value found in the present work.

Even with its apparent geometrical simplicity, a non-trivial magnetic behavior is observed in the dimers. A surprisingly enhanced MAE is obtained for the Pt<sub>2</sub> dimer: 21.64 meV/atom while a reduced MAE is observed for Co<sub>2</sub>. This behavior is due to the different strengths of spin-orbit coupling in Co and Pt which are 3d(5d) transition-metal elements respectively. This fact can be clearly appreciated in the CoPt dimer where the interplay between the competing spin-orbit interactions of both elements yields a modest MAE value (0.4 meV/atom). The easy axis of magnetization is along the bonding axis for the three dimers. The spin moment increases upon Co substitution from 0.88 to 1.93  $\mu_B$ . The giant MAE in Pt<sub>2</sub> can be associated with the development of a large orbital moment which amounts to 1.37  $\mu_B$ .

### Trimers

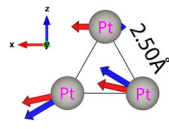
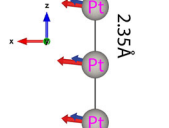
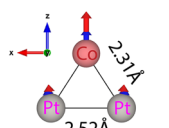
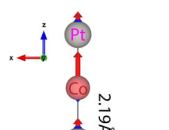
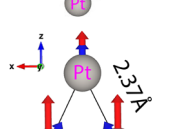
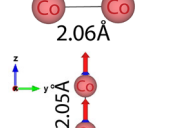
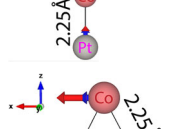
In the case of trimers, the linear chain, as well as the equilateral, isosceles (acute and obtuse) triangles are considered starting structures during geometry optimization. The results regarding structural stability and magnetic properties for the trimers are summarized in Table 2. We found as a general trend triangular ground-state structures, i.e., isosceles triangles for clusters having Co content and an equilateral triangle for Pt<sub>3</sub>. The closest isomers for the clusters at different Co contents are also shown. In the case of the Pt<sub>3</sub> triangle, the obtained bond length is  $d = 2.5$  Å with

**Table 1** Electronic and magnetic properties of Co, Pt, and Co–Pt dimers

Dimer	$E_B$	$\bar{\mu}_x^S$	$\bar{\mu}_y^S$	$\bar{\mu}_z^S$	$\bar{\mu}_x^L$	$\bar{\mu}_y^L$	$\bar{\mu}_z^L$	$M_{\text{easy}}$	$M_{\text{hard}}$	MAE
 Pt <sub>2</sub>	1.690	0.7	–	0.88	0.41	–	1.37	z	x	21.64
 CoPt	1.724	1.38	–	1.4	0.13	–	0.77	z	x	0.4
 Co <sub>2</sub>	1.470	1.93	–	1.93	0.15	–	0.34	z	x	2.67

Results are given for the binding energy  $E_B$  (in eV/atom), equilibrium bond distance,  $d_e$  in Å, average magnetic spin and orbital moments per atom  $\bar{\mu}_\delta^S$  and  $\bar{\mu}_\delta^L$  (in  $\mu_B/\text{atom}$ ), along the different axes of magnetization  $\delta = (x, y, z)$  including the spin-orbit interaction. Additionally, the easy(hard) axes of magnetization and magnetic anisotropy energy per atom(MAE, in meV/atom) between the easy and hard magnetic directions are also shown

**Table 2** Structural, electronic, and magnetic properties of CoPt trimers

Trimer	$E_B$	$\mu_x$	$\mu_y$	$\mu_z$	$L_x$	$L_y$	$L_z$	$S_{\text{easy}}$	$S_{\text{hard}}$	MAE
 Pt <sub>3</sub>	2.194	0.51	0.04	0.51	0.37	0.01	0.37	xy	y	0.78
 Pt <sub>3</sub>	2.111	0.73	—	1.14	0.29	—	0.66	x	z	29.32
 CoPt <sub>2</sub>	2.281	0.94	0.92	0.93	0.22	0.05	0.23	z	x	1.69
 CoPt <sub>2</sub>	2.197	1.40	—	1.30	0.29	—	0.14	z	x	1.02
 Co <sub>2</sub> Pt	2.166	1.73	1.71	1.71	0.22	0.11	0.22	z	y	0.43
 Co <sub>2</sub> Pt	1.919	1.76	—	1.84	0.21	—	0.33	z	x	6.22
 Co <sub>3</sub>	1.809	2.09	2.11	2.08	0.23	0.11	0.15	x	y	2.00

Results are given for the binding energy  $E_B$  (in eV/atom), equilibrium bond distance  $d_e$  (in Å), and local average magnetic spin and orbital moments  $\mu_S^i$  and  $\mu_L^i$  (in  $\mu_B$ ), along the different axes of magnetization including the spin-orbit interaction. Additionally, the magnetic anisotropy energy (MAE, in meV/atom) between the easy and hard magnetic directions is also shown

an average spin magnetic moment of  $\bar{\mu} = 0.51\mu_B$  along the easy axis ( $x$ -axis) in agreement with previous calculations (Błoński et al. 2011). Notice that this trimer exhibits a non-collinear magnetic arrangement between both spin and orbital moments (see Table 2) with meaningful local orbital moments ( $\sim 0.37\mu_B$ ) but a reduced net total magnetic moment due to the non-collinearity. Non-magnetic similar structures were found by other methods (Xiao and Wang 2004; Yang et al. 1997) with bond distances ranging from

2.47 to 2.58 Å. The next excited state is the linear chain from which one finds a shorter bond length  $d = 2.35$  Å and larger magnetic moments ( $\bar{\mu} = 0.73\mu_B$ ). A closer inspection shows slightly larger values of the magnetic moment at the central atom in comparison with the atoms at the edges but it continues showing a non-collinear texture between the spin and orbital moments. This is mainly a consequence of a charge transfer of the  $d$  electrons from the central atom to the other two atoms.

A single Co substitution (CoPt<sub>2</sub>) yields the isosceles triangle to be the ground-state structure with interatomic distances of  $d_{\text{PtPt}} = 2.52 \text{ \AA}$  and  $d_{\text{CoPt}} = 2.31 \text{ \AA}$  respectively. The first excited structure is the linear chain with a central Co atom and two Pt atoms at the edges. Notice, that in this case, the Co–Pt bond length is quite shorter ( $d_{\text{PtCo}} = 2.19 \text{ \AA}$ ) in comparison with the Co–Pt distances found in the Pt<sub>3</sub> linear chain (2.35 Å) and the CoPt<sub>2</sub> triangle (2.31 Å). Further Co substitution (Co<sub>2</sub>Pt) in the isosceles triangle structure prevails as the ground-state but the Co–Co bond is the shortest  $d_{\text{CoCo}} = 2.06 \text{ \AA}$ . The linear chain isomer of the Co<sub>2</sub>Pt cluster favors the Co–Co bond having large magnetic moments. Finally, for Co<sub>3</sub> the lowest energy structure is also an isosceles triangle with two bonds  $d = 2.07 \text{ \AA}$  and  $d = 2.25 \text{ \AA}$ . Other DFT calculations (Fan et al. 1997; Castro et al. 1997) yield the same structure with similar bond distances 2.12–2.43 Å and 2.19–2.25 Å. Concerning the composition dependence of the binding energy,  $E_B$ , one observes a non-monotonous behavior having the CoPt<sub>2</sub> cluster the largest binding energy. This reflects the fact that the CoPt bonds are the strongest.

The average magnetic spin moment per atom in the trimers is  $\bar{\mu} = 0.51\mu_B$  for Pt<sub>3</sub> and increases with Co content up to  $\bar{\mu} = 2.09\mu_B$  for Co<sub>3</sub>. On the other hand, notice that the local spin magnetic moment in the Pt atoms decreases upon Co doping and reaches its maximum value for Co<sub>2</sub>Pt. In contrast, the orbital moment decreases upon Co substitution from  $0.37 \mu_B$  (Pt<sub>3</sub>) to  $0.11 \mu_B$  (Co<sub>3</sub>) as a result of the weakening of the spin-orbit interaction.

In the pure clusters, the local spin moment is close to  $\bar{\mu}_T$ , which indicates that the spin polarization is dominated by the *d*-electrons and that spill-off contributions are not important. For example, in the case of Co<sub>3</sub>, one finds  $\mu_3 = 1.88\mu_B$  and  $\mu_1 = \mu_2 = 1.94\mu_B$ , the former having the largest number of *d*-holes. In comparison with the dimers, one observes narrower orbital moments with small variations as a function of the Co content but still substantial (0.14–0.3  $\mu_B$ ).

As soon as mixed CoPt bonds are present for intermediate concentrations, the local Co moments are enhanced beyond  $2\mu_B$ . This is mainly due to a charge transfer from Co to Pt (increase of the number of Co *d* holes) as already observed in the dimer. Quantitatively, the local  $\mu_{\text{Co}}$  and  $\mu_{\text{Pt}}$  in mixed trimers are similar,

though somewhat smaller, to the corresponding values in the CoPt dimer.

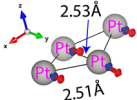
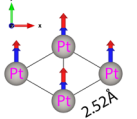
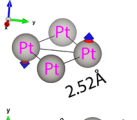
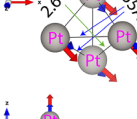
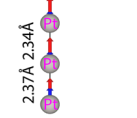
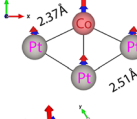
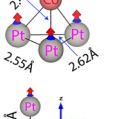
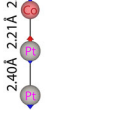
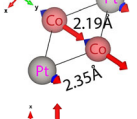
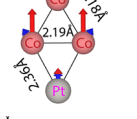
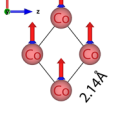
#### Tetramers

Results for the low-lying isomers of the CoPt tetramers are reported in Table 3. The most stable structures (ground and first low-lying isomer) turn out to be rhomboidal-like or distorted tetrahedral geometries. In the case of Pt<sub>4</sub>, we obtain that the optimal structure is a non-planar distorted rhomboid with  $E_B = 2.52 \text{ eV}$  and bond lengths  $d_{\alpha,\beta} = 2.51\text{--}2.53 \text{ \AA}$ . Previous ab initio studies on Pt clusters reported the distorted tetrahedron as the ground-state (Kumar and Kawazoe 2008) structure. In our study, such structure is 39 meV higher in energy than the mentioned ground state. Moreover, such a structure exhibits a non-collinearity between the spin and orbital moments. It is important to mention that including spin-orbit interaction yields to a stabilization of the planar rhombus geometry (Błóński et al. 2011). Thus, the closest isomer is found to be a planar symmetric rhomboid with a bond length of  $d = 2.52$  and  $\Delta E = 8 \text{ meV}$ . It should be noticed that in the case of Pt<sub>4</sub> Xiao and Wang (2004) obtained a rhombus with binding energy  $E_B = 2.62 \text{ eV}$  and for the two bond distances  $d = 2.51, 2.58 \text{ \AA}$ . In contrast, the calculations by Yang et al. (1997) yielded a perfect tetrahedron with  $d = 2.64 \text{ \AA}$  and with binding energy  $E_B = 2.51 \text{ eV}$ .

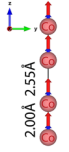
The binding energy shows a non-monotonous dependence on the Pt concentration, which was already found for smaller cluster sizes. In fact, the largest binding energies correspond to the Co<sub>2</sub>Pt<sub>2</sub> and CoPt<sub>3</sub> clusters with  $E_B = 2.76 \text{ eV}$  and  $E_B = 2.66 \text{ eV}$  respectively. Notice that it is in these structures in which the largest number of CoPt bonds are formed. For instance, Co<sub>2</sub>Pt<sub>2</sub> is found to be the most stable of all compositions. It has 4 Co–Pt and 1 Co–Co bonds. Replacing a Pt by a Co atom to obtain Co<sub>3</sub>Pt implies replacing 2 CoPt bonds by two weaker CoCo bonds (see Table 3 for Co<sub>3</sub>Pt). Therefore,  $E_B$  changes significantly. The second most stable cluster is CoPt<sub>3</sub> having 3 Co–Pt and 2 Pt–Pt bonds. In this case, the binding energy of the Pt–Pt bond is close to that of the Co–Pt bond (see the results for the dimer) and as a consequence Co–Pt<sub>3</sub> and Co<sub>2</sub>Pt<sub>2</sub> clusters have similar binding energies.



**Table 3** Structural, electronic, and magnetic properties of CoPt tetramers

Tetramer	$E_B$	$\mu_x$	$\mu_y$	$\mu_z$	$L_x$	$L_y$	$L_z$	$S_{\text{easy}}$	$S_{\text{hard}}$	MAE
Pt <sub>4</sub> 	2.522	0.62	0.70	0.04	0.33	0.35	0.00	y	x	14.80
Pt <sub>4</sub> 	2.520	0.47	0.68	.70	0.30	0.36	0.23	y	x	9.33
Pt <sub>4</sub> 	2.520	0	0	0	0	0	0	z	y	17.57
Pt <sub>4</sub> 	2.483	0.69	0.69, 0	0.69	0.23	0.23, 0	0.23	xy	xyz	2.46
Pt <sub>4</sub> 	2.164	—	0.45	0.76	—	0.25	0.26	z	y	41.08
CoPt <sub>3</sub> 	2.662	1.08	1.06	1.02	0.31	0.37	0.09	y	x	10.08
CoPt <sub>3</sub> 	2.555	0.99	1.01	1.01	0.18	0.25	0.25	yz	x	14.95
CoPt <sub>3</sub> 	2.126	1.03	—	0.72	0.20	—	0.24	z	x	42.19
Co <sub>2</sub> Pt <sub>2</sub> 	2.760	1.38	1.39	1.37	0.23	0.14	0.09	y	z	7.84
Co <sub>3</sub> Pt 	2.499	1.66	1.66	1.66	0.22	0.15	0.15	x	z	2.72
Co <sub>4</sub> 	2.276	2.21	2.21	2.21	0.18	0.10	0.15	x	y	1.37

**Table 3** (continued)

Tetramer	$E_B$	$\mu_x$	$\mu_y$	$\mu_z$	$L_x$	$L_y$	$L_z$	$S_{\text{easy}}$	$S_{\text{hard}}$	MAE
 Co <sub>4</sub>	1.725	2.26	–	2.26	0.18	–	0.29	z	x	1.15

Results are given for the binding energy  $E_B$  (in eV/atom), equilibrium bond distance  $d_e$  (in Å), and local average magnetic spin and orbital moments  $\mu_S^S$  and  $\mu_S^L$  (in  $\mu_B$ ), along the different axes of magnetization including the spin-orbit interaction. Additionally, the magnetic anisotropy energy (MAE, in meV/atom) between the easy and hard magnetic directions is also shown

Concerning the spin magnetic moments, one observes approximately a linear dependence of  $\bar{\mu}_T$  as a function of Pt filling. In general, the substitution of a Co by a Pt atom results in a decrease of  $\Delta\bar{\mu}_T = 0.25$  (see Table 3). The local moments  $\mu_{\text{Co}}$  show the familiar enhancement due to Co-to-Pt *d*-electron charge transfer, which increases the number of *d* holes and allows for the development of  $\mu_{\text{Co}} \simeq 2.1\text{--}2.3\mu_B$ . In addition, the presence of Co in  $\text{Co}_m\text{Pt}_n$  does not produce a significant increase in the local Pt moment (see the results for  $\text{CoPt}_3$  and  $\text{Co}_2\text{Pt}_2$ ). The value of the magnetic moment at the Pt atoms due to the Co proximity is mainly conditioned by charge transfer from Co-to-Pt. Riu-Juan et al. (2007) obtained a very different magnetic behavior for the  $\text{Co}_2\text{Pt}_2$  cluster, in particular for the local moments at the Pt atoms. In fact, in that calculation, the magnetic moments of Pt atoms vanish for the tetrahedral structure and show antiferromagnetic coupling in the rhomboidal structure.

We observe the general trend that the values of the local moments are dominated by the Co-to-Pt charge transfer. Indeed, in contrast to smaller sizes,  $\bar{\mu}_T$  does not increase with increasing Co content (see the results of  $\text{CoPt}_4$  and  $\text{Co}_2\text{Pt}_3$ ). Notice that this particular behavior is mainly due to the electronic characteristics at the Pt atoms. In the case of  $\text{CoPt}_4$ , the charge transfer to the Pt atom is  $\simeq 0.17$  electrons yielding  $\mu_{\text{Pt}} \simeq 0.91\mu_B$  while for  $\text{Co}_2\text{Pt}_3$  the charge transfer to the Pt atoms is larger ( $\simeq 0.46$ ) yielding a smaller  $\mu_{\text{Pt}} \simeq 0.46\mu_B$ . For larger  $\text{Co}_n$  content ( $n > 2$ ), the local Co moments dominate and  $\bar{\mu}_N$  increases monotonically with increasing Co concentration. The ground-state structure of  $\text{Co}_4$  is similar to those found in previous DFT calculations (Fan et al. 1997; Castro et al. 1997; Pereiro et al. 2001; Mlynarski et al. 1999) which is a

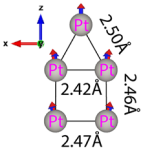
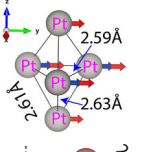
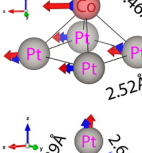
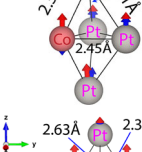
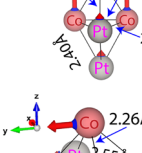
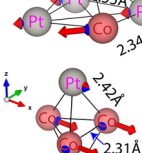
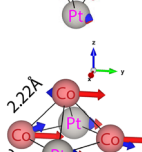
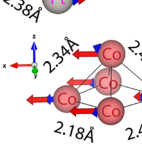
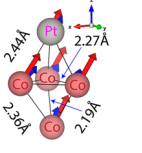

perfect rhomboid structure. The orbital moments continue to provide an important contribution to the total magnetic moment (0.18–0.35  $\mu_B$ )

#### Pentamers

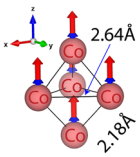
In Table 4, the results for the  $\text{Co}_n\text{Pt}_m$  pentamers are summarized. Although all possible cluster topologies (20 structures) were considered as starting geometries for each composition, only three different correspond to the low-lying isomers. One of them is planar (capped-distorted-square (CDS)) and the other two are three-dimensional and highly coordinated (trigonal bipyramid (TBP) and the square pyramid (SP)). In most cases, the starting low coordinated structures transform into compact structures after the relaxation. The only planar ground-state structure corresponds to  $\text{Pt}_5$  as can be seen in Table 4. Here, we found that the optimal geometry with a binding energy of  $E_B = 2.78$  eV is formed by a distorted square plus an isosceles triangle. This result is in good agreement with previous calculations (Błoński et al. 2011; Kumar and Kawazoe 2008). It is also interesting to note that this structure exhibits a small non-collinearity between the spin and orbital moments with average magnetic moments of  $\bar{\mu}_S = 0.34$  and  $\bar{\mu}_L = 0.27\mu_B$  respectively which are meaningful for a pure Pt structure. Interestingly, three-dimensional structures are formed upon Co doping having more complex magnetic textures as discussed below.

With regard to the structural stability, the binding energy  $E_B$  of the clusters increases monotonously as the number of Co–Pt or Pt–Pt bonds increases reaching the maximum at  $\text{Co}_2\text{Pt}_3$  which has 6 Co–Pt bonds, 2 Pt–Pt bonds, and 1 Co–Co weak bond, then the binding energy decreases upon Co substitution, e.g.,

**Table 4** Electronic and magnetic properties of  $\text{Co}_m\text{Pt}_n$  pentamers

Pentamer	$E_B$	$\bar{\mu}_x^S$	$\bar{\mu}_y^S$	$\bar{\mu}_z^S$	$\bar{\mu}_x^L$	$\bar{\mu}_y^L$	$\bar{\mu}_z^L$	$M_{\text{easy}}$	$M_{\text{hard}}$	MAE
 Pt <sub>5</sub>	2.787	0.24	0.25	0.34	0.16	0.13	0.27	z	x	5.04
 Pt <sub>5</sub>	2.739	0.63	0.56	0.6	0.27	0.19	0.27	y	x	7.21
 CoPt <sub>4</sub>	2.875	1.08	1.09(xy)	1.07	0.23	0.22(xy)	0.26	x	z	3.79
 CoPt <sub>4</sub>	2.871	0.85	0.9	0.94	0.17	0.11	0.23	z	x	9.13
 Co <sub>2</sub> Pt <sub>3</sub>	2.923	1.16	1.1	1.18	0.12	0.08	0.16	z	x	7.99
 Co <sub>2</sub> Pt <sub>3</sub>	2.901	1.32	1.32	1.34	0.15	0.16	0.18	y	z	11.40
 Co <sub>3</sub> Pt <sub>2</sub>	2.900	1.32	1.35	1.33	0.05	0.07	0.12	x	z	2.10
 Co <sub>3</sub> Pt <sub>2</sub>	2.881	1.547	1.531	1.551	0.164	0.135	0.140	y	z	0.67
 Co <sub>4</sub> Pt	2.854	1.78	1.78	1.79	0.14	0.11	0.12	x	z	2.98
 Co <sub>4</sub> Pt	2.713	1.57	1.57	1.57	0.1	0.12	0.13	yz	x	0.75

**Table 4** (continued)

Pentamer	$E_B$	$\bar{\mu}_x^S$	$\bar{\mu}_y^S$	$\bar{\mu}_z^S$	$\bar{\mu}_x^L$	$\bar{\mu}_y^L$	$\bar{\mu}_z^L$	$M_{\text{easy}}$	$M_{\text{hard}}$	MAE
	2.582	2.23	2.23	2.24	0.13	0.13	0.15	z	x	0.13

Results are given for the binding energy  $E_B$  (in eV/atom), average magnetic spin and orbital moments  $\bar{\mu}_\delta^S$  and  $\bar{\mu}_\delta^L$  (in  $\mu_B$ ), along the different axes of magnetization  $\delta = (x, y, z)$  including the spin-orbit interaction. Additionally, the easy(hard) axes of magnetization and magnetic anisotropy energy per atom(MAE, in meV/atom) between the easy and hard magnetic directions are also shown

$\text{Co}_3\text{Pt}_2$  which has 6 Co–Pt bonds and 3 Co–Co bonds. It is important to remark that, in most cases, the excitation energies of the first excited isomers are small ( $\Delta E \simeq 0.01 - 0.03$  eV/atom) since, for each Co concentration, the number of the CoPt or PtPt bonds is very similar (see Table 4).

Regarding the magnetic properties, we observe the general trend that the values of the local spin and orbital moments are dominated by the Co-to-Pt charge transfer. Indeed, in contrast to smaller sizes,  $\bar{\mu}_N$  does not increase with increasing Co content monotonously (see the results for  $\text{CoPt}_4$  and  $\text{Co}_2\text{Pt}_3$  and  $\text{Co}_3\text{Pt}_2$  where  $\bar{\mu}_N$  has a similar same value). Notice that this particular behavior is mainly due to the electronic characteristics at the Pt atoms. In the case of  $\text{CoPt}_4$ , the charge transfer to the Pt atom is  $\simeq 0.17$  electrons yielding  $\mu_{\text{Pt}} \simeq 0.91\mu_B$  while for  $\text{Co}_2\text{Pt}_3$  the charge transfer to the Pt atoms is larger ( $\simeq 0.46$ ) yielding a smaller  $\mu_{\text{Pt}} \simeq 0.46\mu_B$ . For larger  $\text{Co}_n$  content ( $n > 2$ ), the local Co moments dominate and  $\bar{\mu}_N$  increases monotonically with increasing Co concentration. The orbital moments range from  $0.27 \mu_B/\text{atom}$  for  $\text{Pt}_5$  to  $0.15 \mu_B/\text{atom}$  for  $\text{Co}_5$  going through a minimum for  $\text{Co}_3\text{Pt}_2$  ( $0.05 \mu_B/\text{atom}$ ). This is consistent with the interplay between the spin-orbit strength of Pt and Co, since the former yields to strengthen the orbital moment while the latter gives small values.

Larger alloy  $\text{Co}_n\text{Pt}_m$  clusters sizes,  $n + m \leq 9$

In order to obtain further insights regarding the routes of the alloy metal CoPt cluster growing, one needs to explore larger cluster sizes to establish possible trends. Thus, we take larger cluster sizes and consider

$\text{Co}_n\text{Pt}_m$  aggregates having up to 9 atoms. Taking into account both the chemical composition and the magnetic order, as the cluster size increases the number of isomers increases thereof. Therefore, ascertaining the ground-state structure becomes a rather complex and exhaustive task since many low-lying structures with small energy differences between them may coexist. Now that we are interested in providing general bias of the structural and magneto-anisotropy properties of the alloy CoPt clusters, the detailed discussion of all the isomers is beyond the scope of the present study, then the ground-state structure for each cluster size is only discussed.

The ground-state structure for the cluster having six atoms turns to be the  $\text{Co}_2\text{Pt}_4$  aggregate which represents a cluster with a Pt concentration of 67%. Even more, the structural stability seems to be marginally non-affected for Pt concentrations above the 34% ( $m \geq 2$ ), the binding energy as a function of the Pt content shows a plateau-like behavior as it can be appreciated in Fig. 1.

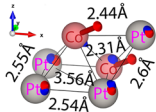
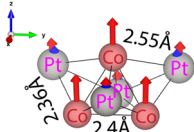
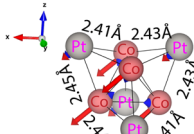
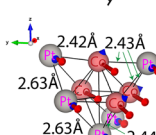
The ground-state structure reflects a tetrahedral symmetry that resembles the three-dimensional square-pyramid structure of the  $\text{Co}_2\text{Pt}_3$  first excited isomer, for what the six-atom cluster can be seen as “extension” of the former structure ( $\text{Co}_2\text{Pt}_3$ ) with one more Pt atom. Notice that the energy difference between the ground-state (trigonal-pyramid structure) and the first low-lying isomer for  $\text{Co}_2\text{Pt}_3$  is rather small, 22 meV/atom only (see Table 4). Slightly smaller distances in the Co–Co bondings (2.3–2.44 Å) compared with the Pt–Pt ones ( $\sim 2.56$  Å) are observed. The average spin magnetic moment amounts to  $1.12 \mu_B$  which is smaller than in the

five-atom cluster due to the “extra” Pt atom while the local orbital moment remains unchanged ( $0.16 \mu_B/\text{atom}$ ). Notice that it exists a small non-collinearity between the spin and orbital moments that was not observed in the five-atom structure. From the seven-atom cluster and larger sizes, it is possible to infer some growing pattern. The clusters form compact core-shell structures keeping the tetragonal symmetry. The Co atoms constitute the core of the cluster while the Pt atoms stay in the outer shell keeping a ratio between Co and Pt close to 50–50%. This growing pattern keeping this rate on its chemical composition has been theoretically predicted for CoPt nanoparticles having larger cluster sizes ( $N = 20–50$  atoms) in which the icosahedral-like structures are expected to pop up (Barcaro et al. 2010). The binding distances and the total magnetic moment of the cluster undergo small variations as a function of the size. The average spin(orbital) moment ranges from 1.13 to 1.37 ( $0.12–0.16$ )  $\mu_B$  respectively as it can be appreciated in Table 5.

### Magnetic anisotropy, orbital moments, and spin reorientation transitions

The magnetic anisotropy (MAE) is, together with the saturation magnetization, one of the main characteristics of any magnetic material. It determines the low-temperature orientation of the magnetic moments with respect to the structure of the system and the stability of the magnetization direction with respect to temperature fluctuations or external fields. These are properties of crucial importance in technological applications such as magnetic recording or memory devices, where one aims to pin the magnetization to a given direction in space. In the following, we present our results regarding spin and orbital magnetic moments of  $\text{Co}_n\text{Pt}_m$  clusters having  $3 \leq n + m \leq 5$  atoms as a function of the Pt content. The average total magnetic moment linearly reduces upon the Pt doping and it occurs in a smoother fashion as the cluster size increases. Figure 2 shows the results for the spin moment  $2\langle S \rangle$  and total moment  $\mu_T = 2\langle S \rangle + \langle L \rangle$

**Table 5** Electronic and magnetic properties of  $\text{Co}_m\text{Pt}_n$  for  $6 \leq n + m \leq 9$

Cluster	$E_B$	$\bar{\mu}_x^S$	$\bar{\mu}_y^S$	$\bar{\mu}_z^S$	$\bar{\mu}_x^L$	$\bar{\mu}_y^L$	$\bar{\mu}_z^L$	MAE
 $\text{Co}_2\text{Pt}_4$	3.267	1.13	1.15	1.12	0.17	0.16	0.14	7.65
 $\text{Co}_3\text{Pt}_4$	3.399	1.17	1.19	1.22	0.17	0.12	0.15	5.86
 $\text{Co}_4\text{Pt}_4$	3.585	1.37	1.37	1.36	0.13	0.13	0.16	2.26
 $\text{Co}_4\text{Pt}_5$	3.645	1.22	1.22	1.23	0.16	0.16	0.15	2.91

Results are given for the binding energy  $E_B$  (in eV/atom), average magnetic spin and orbital moments  $\bar{\mu}_\delta^S$  and  $\bar{\mu}_\delta^L$  (in  $\mu_B$ ), along the different axes of magnetization  $\delta = (x, y, z)$  including the spin-orbit interaction. Additionally, the easy(hard) axes of magnetization and magnetic anisotropy energy per atom (MAE, in meV/atom) between the easy and hard magnetic directions are also shown

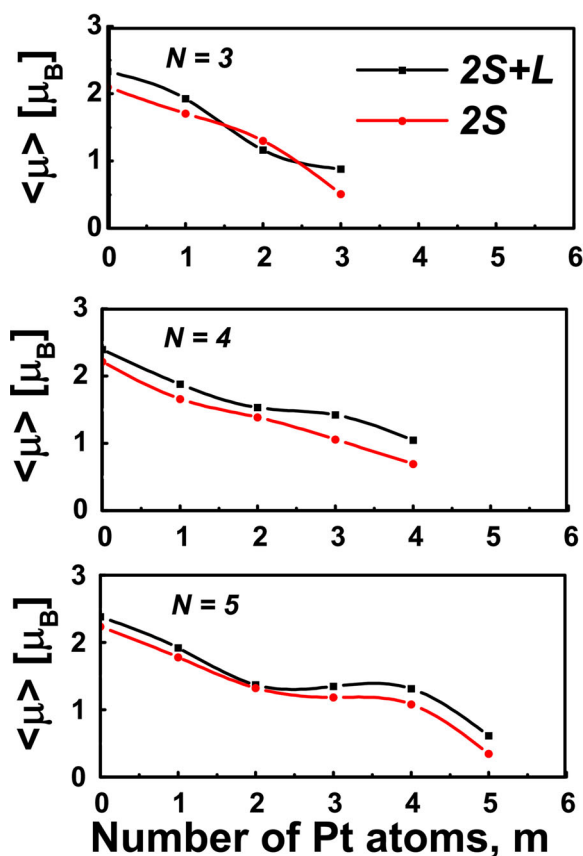


**Fig. 2** Spin moments  $2\langle S \rangle$  and total magnetic moments  $2\langle S \rangle + \langle L \rangle$  of  $Co_nPt_m$  having  $3 \leq n + m \leq 5$  atoms as a function of Pt doping  $m$

(spin plus orbital) as a function of Pt doping for different cluster sizes. It is also important to notice that the orbital moment  $\langle L \rangle$  contributions to the total moment  $\mu_T = 2\langle S \rangle + \langle L \rangle$  amount to about 15–20% ( $\langle L \rangle = 0.2 - 0.3\mu_B$ ). Significant values of the orbital moment  $\mu_{Pt}^L$  at the Pt atoms are usually obtained (0.3–0.6  $\mu_B$ ).

In Fig. 3, the MAE of  $Co_nPt_m$ ,  $n + m \leq 9$  for the clusters is shown. The results correspond to the optimal structures discussed in the previous section. First, notice the remarkable large values of the obtained MAE's for Pt-rich clusters (up to 22 meV/atom for  $Pt_2$ ) and modest values for the Co-rich aggregates (MAE = 2.67 meV/atom for  $Co_2$ ). Second, a disperse concentration dependence is observed for the mixed and pure Pt clusters. Interestingly, robust MAE values are found for the larger clusters sizes ( $N \geq 6$  atoms), 7.65 meV/atom and 5.86 meV/atom for  $Co_2Pt_4$  and  $Co_3Pt_4$  respectively, then it reduces to 2.26 meV/atom and 2.91 meV/atom for  $Co_4Pt_4$  and  $Co_3Pt_5$ . The pure

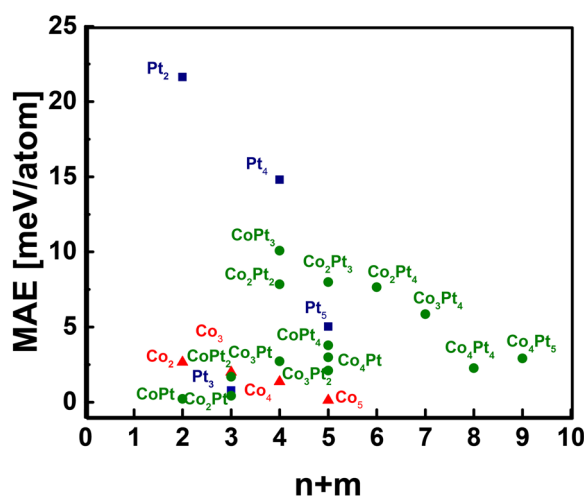


**Fig. 3** Magnetic anisotropy energy of  $Co_nPt_m$  ( $n + m \leq 9$ ) as a function of Pt doping  $m$  for the ground-state structures. The MAE is calculated as the difference in energy between the easy and hard axis of magnetization which is different for each cluster (see Tables 1, 2, 3, 4, and 5)

Co aggregates exhibit a smoother cluster-size dependence together with smaller variations in the MAE behavior (0.13–2.67) meV/atom. Moreover, the same interesting spin-reorientation transitions are observed while increasing the cluster size. By analyzing the ground-state structures, one can observe an alternating easy axis of magnetization for  $Co_nPt_m \geq 3$  from the Z direction to Y direction of magnetization. The spin-reorientation transitions also can be observed in a cluster of a given size as a function of the Pt doping. For instance, for  $N = 5$ , from pure Co ( $m = 0$ ) the MAE oscillates and alternates the direction of magnetization (easy axis) changes from Z direction to the X direction (see Table 4). Spin reorientation transitions are also observed in smaller cluster sizes (e.g., from  $N = 3$  and  $N = 4$ ). The easy-axis direction is the result of different competing interactions (exchange, spin-orbit strength), chemical order, and geometrical structure symmetry, thus a simple a priori estimation is not possible. For instance, canted-easy axes of magnetization are found for clusters having  $6 \leq N \leq 9$  atoms.

Nevertheless, the microscopic origin of the large values of the MAE ( $m = 3$  for  $N = 4$ ,  $m = 3$  for  $N = 5$  or  $m = 4$  for  $N = 6$ ) can be clarified by analyzing the number of CoPt or PtPt bonds having large magnetic moments at the Pt atoms (e.g.,  $\approx 0.91\mu_B$  for  $N = 5$  and  $m = 3$ ) which are the largest for these clusters. Notice that this trend is also followed by the binding

energy. One concludes that the Pt magnetic moments, which are induced by the adjacent Co moments, and the associated spin-orbit interactions at the interface Pt atoms are probably the most important microscopic source of the giant MAE observed in  $\text{Co}_n\text{Pt}_m$ . One therefore expects that reducing the cluster dimensions and the coordination number (open structures) the MAE should increase significantly due to the increase of the moments at the Pt atoms. This can clearly be observed in the case of  $\text{Pt}_3$  and  $\text{Pt}_4$  linear chains having MAEs of 29 and 41 meV/atom respectively.

## Conclusions

In conclusion, a comprehensive study regarding the magneto-electronic properties was performed in small alloy CoPt clusters having  $N \leq 9$  atoms. In particular, the MAE shows a non-monotonous and non-trivial dependence as a function of chemical composition and cluster size that opens new possibilities of tailoring their magnetic behavior in functionalized materials for specific applications. Besides unraveling the ground-state structures together with identifying easy and hard magnetization axes and quantifying the strength of the MAE, the results revealed remarkable multi-axial behaviors and discontinuous spin-reorientation transitions, which depend critically on the cluster composition and dimensionality. Moreover, a growing pattern can be identified showing a tendency to form planar structures for small clusters ( $N \leq 4$ ) and three-dimensional compact core-shell structures for larger sizes. The observed trends and the microscopic understanding derived in this work are expected to shed some light on the magneto-anisotropic properties of CoPt alloys in the range of relevant sizes for the applications. For instance, it should be possible to control and optimize the spin and orbital moments, their order, and magnetic anisotropy by varying the 3d/5d content as well as the distribution of the components within the clusters.

**Acknowledgments** It is a pleasure to thank Prof. Dr. Jesús G. Dorantes-Dávila for helpful discussions and useful comments. The authors thankfully acknowledge the computer resources, technical expertise, and support provided by the Laboratorio Nacional de Supercomputo del Sureste de México (LNS). One of the authors (PRD) acknowledges support from CONACyT Mexico (Grant No.256132). The authors also thank J. Rentería-Arriaga and J.C. Sánchez-Leaños for their technical support.

## Compliance with ethical standards

**Conflict of interest** The authors declare that they have no conflict of interest.

## References

- Airola MB, Morse MD (2002) Rotationally resolved spectroscopy of Pt2. *J Chem Phys* 116(4):1313–1317. Retrieved from <https://doi.org/10.1063/1.1428753>
- Anton J, Jacob T, Fricke B, Engel E (2002) Relativistic density functional calculations for Pt2. *Phys Rev Lett* 89:213001. Retrieved from <https://link.aps.org/doi/10.1103/PhysRevLett.89.213001> <https://doi.org/10.1103/PhysRevLett.89.213001>
- Bansmann J, Baker S, Binns C, Blackman J, Buecher J-P, Dorantes-Dávila J, Dupuis V, Favre L, Kechrakos D, Kleibert A, Meiwes-Broer K-H, Pastor GM, Perez A, Toulemonde O, Trohidou KN, Tuaille J, Xie Y (2005). Magnetic and structural properties of isolated and assembled clusters. *Surface Science Reports*, 56(6), Retrieved from <http://www.sciencedirect.com/science/article/pii/S0167572904001128> [https://doi.org/10.1016/S0167-5729\(04\)00112-8](https://doi.org/10.1016/S0167-5729(04)00112-8)
- Barcaro G, Ferrando R, Fortunelli A, Rossi G (2010) Exotic supported CoPt nanostructures: From clusters to wires. *J Phys Chem Lett* 1(1):111–115. Retrieved from <https://doi.org/10.1021/jz900076m>
- Barden CJ, Rienstra-Kiracofe JC, Schaefer HF (2000) Homonuclear 3d transition-metal diatomics: A systematic density functional theory study. *J Chem Phys* 113(2):690–700. Retrieved from <https://doi.org/10.1063/1.481916>
- Blöchl PE (1994) Projector augmented-wave method. *Phys Rev B* 50:17953–17979. Retrieved from <https://link.aps.org/doi/10.1103/PhysRevB.50.17953> <https://doi.org/10.1103/PhysRevB.50.17953>
- Błoński P, Dennler S, Hafner J (2011) Strong spin-orbit effects in small pt clusters: Geometric structure, magnetic isomers and anisotropy. *J Chem Phys* 134(3):034107. Retrieved from <https://doi.org/10.1063/1.3530799>
- Castro M, Jamorski C, Salahub DR (1997) Structure, bonding, and magnetism of small Fe<sub>n</sub>, Fe<sub>n</sub>, and Ni<sub>n</sub> clusters,  $n \leq 5$ . *Chem Phys Lett* 271(1):133–142. Retrieved from <http://www.sciencedirect.com/science/article/pii/S000926149700420X> [https://doi.org/10.1016/S0009-2614\(97\)00420-X](https://doi.org/10.1016/S0009-2614(97)00420-X)
- Dannenber A, Gruner ME, Hucht A, Entel P (2009) Surface energies of stoichiometric FePt and CoPt alloys and their implications for nanoparticle morphologies. *Phys Rev B* 80:245438. Retrieved from <https://link.aps.org/doi/10.1103/PhysRevB.80.245438> <https://doi.org/10.1103/PhysRevB.80.245438>
- Dupuis V, Favre L, Stanescu S, Tuaille-Combes J, Bernstein E, Perez A (2004) Magnetic assembled nanostructures from pure and mixed Co-based clusters. *J Phys Condensed Matter* 16(22):S2231–S2240. Retrieved from <https://doi.org/10.1088/0953-8984/16/22/024>

- Entel P, Gruner ME (2009) Large-scale ab initio simulations of binary transition metal clusters for storage media materials. *J Phys Condensed Matter* 21(6):064228. Retrieved from <https://doi.org/10.1088/0953-8984/21/6/064228>
- Fan H-J, Liu C-W, Liao M-S (1997) Geometry, electronic structure and magnetism of small Co ( $n = 2-8$ ) clusters. *Chem Phys Lett* 273(5):353–359. Retrieved from <http://www.sciencedirect.com/science/article/pii/S0009261497005344> [https://doi.org/10.1016/S0009-2614\(97\)00534-4](https://doi.org/10.1016/S0009-2614(97)00534-4)
- Favre L, Dupuis V, Bernstein E, Mélinon P, Pérez A, Stanesco S, Hodeau J-L (2006) Structural and magnetic properties of CoPt mixed clusters. *Phys Rev B* 74:14439. Retrieved from <https://link.aps.org/doi/10.1103/PhysRevB.74.014439> <https://doi.org/10.1103/PhysRevB.74.014439>
- Feng R-J, Xu X-H, Wu H-S (2007) Electronic structure and magnetism in (CoPt) $n$  ( $n \leq 5$ ) clusters. *J Magn Magn Mater* 308(1):131–136. Retrieved from <http://www.sciencedirect.com/science/article/pii/S030488530600864X> <https://doi.org/10.1016/j.jmmm.2006.05.012>
- Gambardella P, Rusponi S, Veronese M, Dhesi SS, Grazioli C, Dallmeyer A, Brune H (2003) Giant magnetic anisotropy of single cobalt atoms and nanoparticles. *Science* 300(5622):1130–1133. Retrieved from <https://science.sciencemag.org/content/300/5622/1130> <https://doi.org/10.1126/science.1082857>
- Gradmann U (1993) Chapter 1 magnetism in ultrathin transition metal films. In: (vol 7, pp 1–96). Elsevier. Retrieved from <http://www.sciencedirect.com/science/article/pii/S1567271905800423> [https://doi.org/10.1016/S1567-2719\(05\)80042-3](https://doi.org/10.1016/S1567-2719(05)80042-3)
- Gruner ME, Entel P (2009) Simulating functional magnetic materials on supercomputers. *Journal of Physics: Condensed Matter* 21(29):293201. Retrieved from <https://doi.org/10.1088/0953-8984/21/29/293201>
- Gruner ME, Rollmann G, Entel P, Farle M (2008) Multiply twinned morphologies of FePt and CoPt nanoparticles. *Phys Rev Lett* 100:087203. Retrieved from <https://link.aps.org/doi/10.1103/PhysRevLett.100.087203> <https://doi.org/10.1103/PhysRevLett.100.087203>
- Hales DA, Su C, Lian L, Armentrout PB (1994) Collision-induced dissociation of Co $_n$  ( $n=2-8$ ) with Xe: Bond energies of cationic and neutral cobalt clusters, dissociation pathways, and structures. *J Chem Phys* 100(2):1049–1057. Retrieved from <https://doi.org/10.1063/1.466636>
- Hellwig O, Berger A, Thomson T, Dobisz E, Bandic ZZ, Yang H, Fullerton EE (2007) Separating dipolar broadening from the intrinsic switching field distribution in perpendicular patterned media. *Appl Phys Lett* 90(16):162516. Retrieved from <https://doi.org/10.1063/1.2730744>
- Henkelman G, Arnaldsson A, Jónsson H (2006) A fast and robust algorithm for bader decomposition of charge density. *Comput Mater Sci* 36(3):354–360. <https://doi.org/10.1016/j.commatsci.2005.04.010>
- Hohenberg P, Kohn W (1964) Inhomogeneous electron gas. *Phys Rev* 136:B864–B871. Retrieved from <https://link.aps.org/doi/10.1103/PhysRev.136.B864> <https://doi.org/10.1103/PhysRev.136.B864>
- Jamet M, Négrier M, Dupuis V, Tuillon-Combes J, Mélinon P, Pérez A, Bagueard B (2001) Interface magnetic anisotropy in cobalt clusters embedded in a platinum matrix. *J Magn Magn Mater* 237(3):293–301. Retrieved from <http://www.sciencedirect.com/science/article/pii/S0304885301006953> [https://doi.org/10.1016/S0304-8853\(01\)00695-3](https://doi.org/10.1016/S0304-8853(01)00695-3)
- Knickerbein MB (2007) Magnetic moments of small bimetallic clusters: ConMn. *Phys Rev B* 75:014401. Retrieved from <https://link.aps.org/doi/10.1103/PhysRevB.75.014401> <https://doi.org/10.1103/PhysRevB.75.014401>
- Kohn W, Sham LJ (1965) Retrieved from <https://link.aps.org/doi/10.1103/PhysRev.140.A1133> <https://doi.org/10.1103/PhysRev.140.A1133>. *Phys Rev* 140:A1133–A1138
- Kresse G, Furthmüller J (1996) Efficient iterative schemes for ab initio total-energy calculations using a plane-wave basis set. *Phys Rev B* 54:11169–11186. Retrieved from <https://link.aps.org/doi/10.1103/PhysRevB.54.11169> <https://doi.org/10.1103/PhysRevB.54.11169>
- Kresse G, Hafner J (1993) Ab initio molecular dynamics for liquid metals. *Phys Rev B* 47:558–561. Retrieved from <https://link.aps.org/doi/10.1103/PhysRevB.47.558> <https://doi.org/10.1103/PhysRevB.47.558>
- Kresse G, Joubert D (1999) From ultrasoft pseudopotentials to the projector augmented-wave method. *Phys Rev B* 59:1758–1775. Retrieved from <https://link.aps.org/doi/10.1103/PhysRevB.59.1758> <https://doi.org/10.1103/PhysRevB.59.1758>
- Kumar V, Kawazoe Y (2008) Evolution of atomic and electronic structure of Pt clusters: Planar, layered, pyramidal, cage, cubic, and octahedral growth. *Phys Rev B* 77:205418. Retrieved from <https://link.aps.org/doi/10.1103/PhysRevB.77.205418> <https://doi.org/10.1103/PhysRevB.77.205418>
- Kumbhar A, Spinu L, Agnoli F, Wang K, Zhou W, O'Connor CJ (2001) Magnetic properties of cobalt and cobalt-platinum alloy nanoparticles synthesized via microemulsion technique. *IEEE Trans Magn* 37(4):2216–2218. <https://doi.org/10.1109/20.951128>
- Liou SH, Huang S, Klimek E, Kirby RD, Yao YD (1999) Enhancement of coercivity in nanometer-size CoPt crystallites. *J Appl Phys* 85(8):4334–4336. Retrieved from <https://doi.org/10.1063/1.370359>
- Maret M, Cadeville M, Poinso R, Herr A, Beaurepaire E, Monier C (1997) Structural order related to the magnetic anisotropy in epitaxial (111) CoPt $_3$  alloy films. *J Magn Magn Mater* 166(1):45–52. Retrieved from <http://www.sciencedirect.com/science/article/pii/S0304885396004532> [https://doi.org/10.1016/S0304-8853\(96\)00453-2](https://doi.org/10.1016/S0304-8853(96)00453-2)
- Maret M, Cadeville M, Staiger W, Beaurepaire E, Poinso R, Herr A (1996) Retrieved from <http://www.sciencedirect.com/science/article/pii/0040609095070494> [https://doi.org/10.1016/0040-6090\(95\)07049-4](https://doi.org/10.1016/0040-6090(95)07049-4). *Thin Solid Films* 275(1):224–227
- Mermin ND (1965) Thermal properties of the inhomogeneous electron gas. *Phys Rev* 137:A1441–A1443. Retrieved from <https://link.aps.org/doi/10.1103/PhysRev.137.A1441> <https://doi.org/10.1103/PhysRev.137.A1441>



- Plumer ML, van Ek DWJ (2001) The physics of ultra-high-density magnetic recording (Vol. 41). Springer-Verlag, Berlin. <https://doi.org/10.1007/978-3-642-56657-8>
- Moskovkin P, Pisov S, Hou M, Raufast C, Tournus F, Favre L, Dupuis V (2007) Model predictions and experimental characterization of Co-Pt alloy clusters. *Eur Phys J D* 43:27–32. Retrieved from <https://doi.org/10.1140/epjd/e2007-00066-0>
- Muñoz-Navia M, Dorantes-D'ávila J, Zitoun D, Amiens C, Jaouen N, Rogalev A, Pastor GM (2009) Tailoring the magnetic anisotropy in CoRh nanoalloys. *Appl Phys Lett* 95(23):233107. Retrieved from <https://doi.org/10.1063/1.3272000>
- Mlynarski P, Iglesias M, Pereiro M, Baldomir D, Wojtczak L (1999) Properties and structure of small cobalt clusters: Nonlocal density functional calculations. *Vacuum* 54(1):143–149. Retrieved from <http://www.sciencedirect.com/science/article/pii/S0042207X98004503> [https://doi.org/10.1016/S0042-207X\(98\)00450-3](https://doi.org/10.1016/S0042-207X(98)00450-3)
- Penuelas J, Ouerghi A, Andrezza-Vignolle C, Gierak J, Bourhis E, Andrezza P, Sauvage T (2009) Local tuning of CoPt nanoparticle size and density with a focused ion beam nanowriter. *Nanotechnology* 20(42):425304. Retrieved from <https://doi.org/10.1088/0957-4484/20/42/425304>
- Perdew JP, Burke K, Wang Y (1996) Generalized gradient approximation for the exchange-correlation hole of a many-electron system. *Phys Rev B* 54:16533–16539. Retrieved from <https://link.aps.org/doi/10.1103/PhysRevB.54.16533> <https://doi.org/10.1103/PhysRevB.54.16533>
- Perdew JP, Chevary JA, Vosko SH, Jackson KA, Pederson MR, Singh DJ, Fiolhais C (1992) Atoms, molecules, solids, and surfaces: Applications of the generalized gradient approximation for exchange and correlation. *Phys Rev B* 46:6671–6687. Retrieved from <https://link.aps.org/doi/10.1103/PhysRevB.46.6671> <https://doi.org/10.1103/PhysRevB.46.6671>
- Pereiro M, Man'kovsky S, Baldomir D, Iglesias M, Mlynarski P, Valladares M, Arias JE (2001) Model potential nonlocal density functional calculations of small cobalt clusters,  $\text{Co} \leq 5$ . *Comput Mater Sci* 22(1):118–122. Retrieved from <http://www.sciencedirect.com/science/article/pii/S092702560100177X> [https://doi.org/10.1016/S0927-0256\(01\)00177-X](https://doi.org/10.1016/S0927-0256(01)00177-X)
- Rollmann G, Sahoo S, Hucht A, Entel P (2008) Magnetism and chemical ordering in binary transition metal clusters. *Phys Rev B* 78:134404. Retrieved from <https://link.aps.org/doi/10.1103/PhysRevB.78.134404> <https://doi.org/10.1103/PhysRevB.78.134404>
- Ruiz-Díaz P, Muñoz-Navia M, Dorantes-D'ávila J, Ruiz-Dí P (2018) Charge-doping and chemical composition-driven magnetocrystalline anisotropy in CoPt core-shell alloy clusters. *J Nanopart Res* 20:58. Retrieved from <https://link.springer.com/article/10.1007/s11051-018-4164-z> <https://doi.org/10.1007/s11051-018-4164-z>
- Sahoo S, Hucht A, Gruner ME, Rollmann G, Entel P, Postnikov A, Sil S (2010) Magnetic properties of small pt-capped fe, co, and ni clusters: A density functional theory study. *Phys Rev B* 2:054418. Retrieved from <https://link.aps.org/doi/10.1103/PhysRevB.82.054418> <https://doi.org/10.1103/PhysRevB.82.054418>
- Sanville E, Kenny SD, Smith R (2007) Improved grid-based algorithm for bader charge allocation. *J Computa Chem* 28(5):899–908. Retrieved from <https://onlinelibrary.wiley.com/doi/abs/10.1002/jcc.20575> <https://doi.org/10.1002/jcc.20575>
- Shaw JM, Rippard WH, Russek SE, Reith T, Falco CM (2007) Origins of switching field distributions in perpendicular magnetic nanodot arrays. *J Appl Phys* 101(2):023909. Retrieved from <https://doi.org/10.1063/1.2431399>
- Sun S, Murray CB, Weller D, Folks L, Moser A (2000) Monodisperse FePt nanoparticles and ferromagnetic FePt nanocrystal superlattices. *Science* 287(5460):1989–1992. Retrieved from <https://science.sciencemag.org/content/287/5460/1989> <https://doi.org/10.1126/science.287.5460.1989>
- Tamion A, Hillenkamp M, Tournus F, Bonet E, Dupuis V (2009) Accurate determination of the magnetic anisotropy in cluster-assembled nanostructures. *Appl Phys Lett* 95(6):062503. Retrieved from <https://doi.org/10.1063/1.3200950>
- Tang W, Sanville E, Henkelman G (2009) Retrieved from <https://doi.org/10.1088/0953-8984/21/8/084204>. *Journal of Physics: Condensed Matter* 21(8):084204
- Thomson T, Hu G, Terris BD (2006) Intrinsic distribution of magnetic anisotropy in thin films probed by patterned nanostructures. *Phys Rev Lett* 96:257204. Retrieved from <https://link.aps.org/doi/10.1103/PhysRevLett.96.257204> <https://doi.org/10.1103/PhysRevLett.96.257204>
- Valvidares SM, Dorantes-Dávila J, Isern H, Ferrer S, Pastor GM (2010) Interface-driven manipulation of the magnetic anisotropy of ultrathin co films on Pt(111): Substrate deposition of hydrogen and model calculations. *Phys Rev B* 81:024415. Retrieved from <https://doi.org/10.1103/PhysRevB.81.024415>
- Vaz CAF, Bland JAC, Lauhoff G (2008) Magnetism in ultrathin film structures. *Reports Progr Phys* 71(5):056501. Retrieved from <https://doi.org/10.1088/0034-4885/71/5/056501>
- Vita AD, Gillan MJ (1992) The energetics of hydrogen in aluminium calculated from first principles. *Journal of Physics: Condensed Matter* 4(2):599–611. Retrieved from <https://doi.org/10.1088/0953-8984/4/2/028>
- Xiao L, Wang L (2004) Structures of Platinum clusters: Planar or spherical. *J Phys Chem A* 108(41):8605–8614. Retrieved from <https://doi.org/10.1021/jp0485035>
- Yanagisawa M, Shiota N, Yamaguchi H, Suganuma Y (1983) Corrosion-resisting co-pt thin film medium for high density recording. *IEEE Trans Magn* 19(5):1638–1640. <https://doi.org/10.1109/TMAG.1983.1062738>
- Yang SH, Drabold DA, Adams JB, Ordejón P, Glassford K (1997) Density functional studies of small platinum clusters. *Journal of Physics: Condensed Matter* 9(5):L39–L45. Retrieved from <https://doi.org/10.1088/0953-8984/9/5/002>
- Yin S, Moro R, Xu X, de Heer WA (2007) Magnetic enhancement in cobalt-manganese alloy clusters. *Phys Rev Lett*

- 98:113401. Retrieved from <https://link.aps.org/doi/10.1103/PhysRevLett.98.113401> <https://doi.org/10.1103/PhysRevLett.98.113401>
- Yu M, Liu Y, Sellmyer DJ (2000) Nanostructure and magnetic properties of composite CoPt:c films for extremely high-density recording. *J Appl Phys* 87(9):6959–6961. Retrieved from <https://doi.org/10.1063/1.372899>
- Zarechnaya E, Skorodumova N, Simak S, Johansson B, Isaev E (2008) Theoretical study of linear monoatomic nanowires, dimer and bulk of Cu, Ag, Au, Ni, Pd and Pt. *Comput Mater Sci* 43(3):522–530. Retrieved from <http://www.sciencedirect.com/science/article/pii/S0927025608000037> <https://doi.org/10.1016/j.commatsci.2007.12.018>
- Zitoun D, Respaud M, Fromen M-C, Casanove MJ, Lecante P, Amiens C, Chaudret B (2002) Magnetic enhancement in nanoscale corh particles. *Phys Rev Lett* 89:n. Retrieved from <https://link.aps.org/doi/10.1103/PhysRevLett.89.037203> <https://doi.org/10.1103/PhysRevLett.89.037203>

**Publisher's note** Springer Nature remains neutral with regard to jurisdictional claims in published maps and institutional affiliations.